

# Magnetic Anisotropy of Isolated Cobalt Nanoplatelets

T.O. Strandberg and C.M. Canali

*Division of Physics, Department of Chemistry and Biomedical Sciences, Kalmar University, 391 82 Kalmar, Sweden\**

A.H. MacDonald

*Department of Physics, University of Texas at Austin, Austin TX 78712*

(Date textdate)

Motivated in part by experiments performed by M.H. Pan *et Al.* [1], we have undertaken a theoretical study of the the magnetic properties of two-monolayer thick Co nanoplatelets with an equilateral triangular shape. The analysis is carried out using a microscopic Slater-Koster tight-binding model with atomic exchange and spin-orbit interactions designed to realistically capture the salient magnetic features of large nanoclusters [2] containing up to 350 atoms. Two different geometries of the FCC lattice are studied, in which the nanoplatelet surface is aligned parallel to the FCC (111) and (001) crystal planes respectively. We find that the higher coordination number in the (111) truncated crystal is more likely to reproduce the perpendicular easy direction found in experiment. Qualitatively, the most important parameter governing the anisotropy of the model is found to be the value of the intra-atomic exchange integral  $J$ . If we set the value of  $J$  near the bulk value in order to reproduce the experimentally observed magnitude of the magnetic moments, we find both quasi-easy-planes and perpendicular easy directions. At larger values of  $J$  we find that the easy-axis of magnetization is perpendicular to the surface, and the value of the magnetic anisotropy energy per atom is larger. The possible role of hybridization with substrate surface states in the experimental systems is discussed.

## I. INTRODUCTION

The magnetic properties of transition metal nanostructures are very distinct from those of bulk materials [3, 4]. Typically, the magnetic moment is enhanced at surfaces [5], in ultra-thin magnetic films [6, 7], and in magnetic nanoparticles and clusters [8, 9, 10, 11], due to lowered symmetry and reduced coordination at the surface. Similarly, one of the most phenomenologically important properties of magnetic materials, the magnetic anisotropy energy (MAE) is considerably altered in systems of reduced dimensionality. For example, the magnetic anisotropy per atom in two-dimensional (2D) monolayers is more than one order of magnitude larger than in bulk [12]. In one-dimensional (1D) magnetic chains the enhancement is two to three orders of magnitude [12]. It is therefore reasonable to expect that quasi zero-dimensional nanostructures, that is to say ultra-small nanoparticles and nanoclusters, should display even more strongly enhanced anisotropy and other novel phenomena [13].

The study of magnetic nanoparticles has a long history that goes back to the work of Neel [14] and Stoner and Wohlfart [15]. However, it is only in recent years that it has been possible to perform experiments on a single magnetic nanoparticle [16], and to assemble on

a metal surface monolayer magnetic clusters containing up to a few tens of atoms [17]. 2D monolayer clusters of a few atoms deposited on a metal surface display a giant magnetic anisotropy perpendicular to the surface together with unusually large orbital moments [12, 17] which contribute significantly to the total magnetic moment of the system, unlike in the bulk where they are almost totally quenched by electron delocalization and crystal field splitting. Orbital magnetism and magneto-crystalline anisotropy in solids have their common microscopic origin in the spin-orbit interaction. The enhancement of these two properties in nanoclusters, either free or deposited on metallic surface [13], is a fundamental issue in the study of magnetism. Several theoretical calculations based on ab-initio spin-density-functional theory [18, 19] or tight-binding models [20, 21] have either predicted or partly reproduced these experimental results. However a number of important points remain unclear: for example, how the magnetic anisotropy evolves from single-atom to bulk behavior; how it is affected by the atomic magnetic moments, how it depends on the arrangement of the atoms in the cluster and on the surfaces where the cluster is possibly deposited.

From the point of view of applications, the remarkable magnetic properties of transition-metal nanoclusters suggest a potential role as units of ultra-high density magnetic information storage. Unfortunately, despite their large anisotropies per atom, these clusters are still superparamagnetic at room temperature [32]. Since the *total* anisotropy energy scales roughly with cluster size, one could in principle try to increase the anisotropy barrier and hence the blocking temperature, by increasing the cluster size. However, experiment [17] has shown that the MAE per atom of clusters on metal surfaces quickly

---

\*Division of Solid State Theory, Department of Physics, Lund University, SE-223 62 Lund, Sweden

degrades with the number of atoms.

Recently, the group of M.H. Pan *et al.* [1], has created arrays of self-assembled Co clusters on top of a Si (111) surface using epitaxial quantum growth techniques. In order to prevent silicide formation with the Co, the surface is covered with half a monolayer (ML) of Al clusters. The resulting symmetry of the substrate surface prompts the growth of 2 ML thick Co clusters with equilateral triangle shapes and distinct quantized sizes with sides equal to either 2 or 3 times the length of the side of the 7 by 7 Si unit cell - or 5.4 and 8.1 nm, respectively. From the system symmetry and the measured height of the Co clusters, we propose that the Co atoms position themselves so as to form two FCC (111) crystal planes, with a modified lattice constant approximately equal to that of Si.

SQUID magnetometer measurements reveal perpendicular easy directions, and a very high blocking temperature of  $40 \pm 5$  K (corresponding to an anisotropy energy of 90 meV) and  $100 \pm 5$  K (corresponding to an anisotropy energy of 220 meV), respectively. Estimating the number of atoms in the smaller and larger clusters to be 225 and 484 Co atoms each, this translates to anisotropy energies of approximately 0.40 and 0.45 meV per atom, corresponding to values that are one order of magnitude larger than bulk estimates (0.04-0.06 meV/atom [22]). The high anisotropy energy of the Co clusters combined with the Si substrate surface, provides a material that seems ideal for logical circuits integrated with ultra-high-density memory.

The purpose of this paper is to investigate theoretically the magnetic properties of nanoclusters similar to those considered in the experiment of Ref. 1. Using a tight-binding model characterized by short range exchange and atomic spin-orbit interactions, we have modeled these clusters to shed light on the experimentally observed magnitude of the anisotropy energy and the perpendicular easy directions.

We find that when the intra-atomic exchange constant  $J$  (which is a purely phenomenological quantity in our model) is smaller than 1 eV the magnetic moment is in the plane of the nanoplatelet. For larger values of  $J$  - between 1 and 1.5 eV - the easy axis of the magnetization is predominately orthogonal to the plane, and the perpendicular anisotropy energy is in the range of the large values observed in experiment. Associated and closely connected with the enhanced magnetic anisotropy, we find that the orbital magnetic moment is also enhanced and strongly anisotropic, pointing predominantly in the direction of the easy axis. The stabilization of a perpendicular magnetization orientation by enhanced anisotropy of the orbital magnetic moment is likely related to details of the orbital character of states near the Fermi level.

Our motivation for studying the dependence on  $J$  is that the magnetic properties are governed by the ratio of  $J$  to the  $d$ -electron bandwidth  $W_d$ . Epitaxial registration of the Co atoms on the Si/Al surface results in clusters

with an effective lattice constant that is larger than that of bulk Co. This would imply an enhanced value of the ratio  $J/W_d$  which we try to mimic by increasing  $J$  while keeping  $W_d$  constant. In this paper, besides values  $J$  between 1.0 and 1.5 eV, which we believe describe realistically our system, we also study the asymptotic behavior for the non-physical region  $J > 1.5$  eV.

This paper is organized as follows. In section II we outline the theoretical model employed in the analysis and discuss what can and cannot be learned from its output. Section III summarizes the numerical results and the predictions of our model for the magnetic moment, the anisotropy energy landscape and the anisotropy energy per atom as a function of cluster size for two different geometries of the FCC crystal obtained by truncating it along two different crystal planes. In Section IV we investigate the underlying mechanisms responsible for the observed magnetic properties by studying the dependence of the quasi-particle spectrum as a function of the intra-atomic exchange strength  $J$ . We look at the change in orbital character and in the distribution of orbital moments of the quasiparticle eigenstates for increasingly larger values of  $J$ . Finally, in Section V we summarize our conclusions and suggest an alternative configuration of substrate atoms that might produce nanoparticles with interesting magnetic properties.

## II. THEORY

### A. General considerations

Nanoclusters consisting of ferromagnetic transition metal atoms are characterized by an unbalanced spin population and a resulting net magnetization. This paper deals with nanoparticles of sizes below the 10 nm limit, where only a single magnetized domain is observed. The magnetic anisotropy in small ferromagnetic particles comes from two distinct sources. Firstly, the long range magnetic dipole interactions cause a dependence on the overall shape of the particle. Then, there is the short range exchange interaction, that via the spin-orbit (SO) interaction is sensitive to all aspects of the electron hopping network, causing a dependence on crystal symmetry, facet orientation and particle shape. The focus of our model is this so-called magneto-crystalline anisotropy, which is responsible for most of the interesting physics in ferromagnetic particles. The magneto-static shape anisotropy, due to the magnetic dipole interactions, can be added as a separate contribution when it is not negligible.

In an infinite crystal, neighbors of a particular site in the lattice will deform the magnetic electron cloud, which will therefore reflect the point symmetry of the atomic position. The SO interaction then couples the deformed orbitals to the exchange coupled spins. In  $3d$  transition metals, the outer, partially filled  $d$  shells, are strongly affected by the crystalline environment. Elec-

tronic structure calculations [23] imply that most of the anisotropy in this case comes from a competition between an almost completely isotropic on-site exchange interaction and strong inter-atomic hopping. The role of the spin-orbit interaction is that of a relatively small perturbation acting as an mediator between the two.

The quenching of the orbitals in a crystalline environment breaks the rotational invariance at each site, and the orbitals are not free to orient themselves under the influence of an external field. As a result, the atomic wavefunctions are now no longer eigenstates of  $L_z$ . The new eigenstates are instead linear combinations for which the expectation value of  $L_z$  vanishes. In 3d transition metals the crystal field splitting is large and the orbital angular momentum is small. Complete quenching of the wavefunctions is counteracted by the SO interaction. A microscopic derivation of the magnetic anisotropy in ferromagnetic materials is highly non-trivial. The most promising attempts are currently within spin density functional theory.

In a nanoparticle of finite size, the magnetic anisotropy is strongly affected by the presence of symmetry breaking surfaces. The surface dependence is sensed throughout the system by shape dependent inter-atomic electron hopping paths. In nanoclusters, the anisotropy is therefore expected to be much larger than in the bulk, and to depend crucially on the particular shape of the particle. These properties have been confirmed for Co nanoparticles [16].

## B. The model

To construct an effective spin Hamiltonian that describes the exchange interaction in transition metals, we employ a tight-binding model devised by A. Cehovin *et al.* [2]. The aim of this model is to capture generic features of ferromagnetic metal nanoparticles. Our model Hamiltonian takes the following form:

$$\mathcal{H} = \mathcal{H}_{\text{Band}} + \mathcal{H}_{\text{Exc}} + \mathcal{H}_{\text{SO}} + \mathcal{H}_{\text{Zeeman}} \quad (1)$$

Let's address each of the terms in (1), starting from the left. The ferromagnetism of transition metals involves itinerant electrons, which necessitates the use of band theory. The path of the itinerant electrons is governed by  $\mathcal{H}_{\text{Band}}$ , describing the orbital motion of the electrons inside the particle. This is a single-particle tight-binding term, where the on-site energies of the Wannier orbitals and the hopping matrix elements between two of them are parameterized by Slater-Koster parameters [24]. In neutral Co, we use nine orbitals - one 4s, three 4p and five 3d. Including the spin degrees of freedom, there are 18 quasiparticle orbitals per atom in our s-p-d tight-binding model.  $\mathcal{H}_{\text{Band}}$  is given in second quantized form by

$$\mathcal{H}_{\text{Band}} = \sum_{ij} \sum_s \sum_{\mu_1 \mu_2} t_{\mu_1 \mu_2 s}^{ij} c_{i\mu_1 s}^\dagger c_{j\mu_2 s} \quad (2)$$

where  $c^\dagger$  and  $c$  are the creation and annihilation operators, which operate on single-particle states labeled by atomic site ( $ij$ ), the 9 orbitals ( $\mu$ ) and spin ( $s$ ). For the  $t_{\mu_1 \mu_2 s}^{ij}$  we use SK parameters [24] that have been extracted from ab initio calculations for the corresponding bulk systems.

The main purpose of this model is to realistically include the spin-orbit interaction. The exchange part of the Hamiltonian is simplified using a mean-field approximation. We first approximate  $\mathcal{H}_{\text{Exc}}$  including only the ferromagnetic exchange, by simply treating the intra-atomic exchange for  $d$ -orbitals.

$$\mathcal{H}_{\text{Exc}} = -2J \sum_i \vec{S}_{di} \cdot \vec{S}_{di} \quad (3)$$

where

$$\vec{S}_{di} = \sum_{\mu \in d} \vec{S}_{i\mu} = \frac{1}{2} \sum_{\mu \in d} \sum_{ss'} c_{i\mu s}^\dagger \vec{\tau}_{ss'} c_{i\mu s'} \quad (4)$$

and  $J$  is the parameter that determines the strength of the exchange interaction. This is set to 1 eV in order to produce an average magnetic moment per atom of the order of  $2\mu_B$ , somewhat larger than bulk value, in accordance with calculations [25] and experiment [8] [9] for Co nanoclusters.  $\vec{\tau}$  is a three-vector with the Pauli matrices as components. We now simplify the exchange interaction by performing a mean-field decomposition,

$$\vec{S}_{di} = \langle \vec{S}_{di} \rangle + \delta \vec{S}_{di} \quad (5)$$

and dropping the second order fluctuation terms in  $\delta \vec{S}_{di}$ . The ground state  $\langle \vec{S}_{di} \rangle$  is determined self-consistently. We can now diagonalize the Hamiltonian numerically, solving a self-consistency condition iteratively for the mean field order parameters.

Simplifying further still, the exchange mean splitting field is averaged over all sites, forcing all spins to change their orientation coherently.

$$\vec{h}_i \equiv h\hat{\Omega} = \frac{J}{g_s \mu_B} \langle \vec{S}_{di} \rangle \quad (6)$$

This procedure simplifies the anisotropy landscape, neglecting non-collinear spin configurations. These can occur in nanoparticles, but for larger clusters most atoms have the same spin orientations, effectively rendering the system coherent. It is also possible to prepare a nanoparticle so as to display simple coherent magnetization reversal processes [26] [16]. When inserting the bulk values for magnetization and spin-splitting field, the mean-field formula (6) yields the correct value of  $J$ . This serves as a theoretical consistency check, but the motivation for the choice of  $J$  is that it produces the experimental and computed mean moment per atom. Selecting a different  $J$  as input parameter, yields a different self-consistent spin-splitting field. Below we will consider  $J$  as a phenomenological parameter and we will explore how the

magnetic properties of the cluster – in particular, the MAE – depend on its value.

We expect the mean-field approximation (5), (6) to work well, since we are interested only in particles sizes in the coherent mono domain region. Achieving self-consistency in the homogeneous average spin splitting field  $\vec{h}$ , allows for variations around a mean value in charge density and atomic moments. With this simplified model, we are able to study larger clusters, up to sizes of 300-400 atoms, for which the homogeneous exchange field approximation becomes increasingly accurate.

$\mathcal{H}_{SO}$  is of atomic character, representing the spin-orbit interaction [27],

$$\mathcal{H}_{SO} = \xi_d \sum_i \sum_{\mu\mu'} \sum_{ss'} \langle \mu s | \vec{L} \cdot \vec{S} | \mu' s' \rangle c_{i\mu s}^\dagger c_{i\mu' s'} \quad (7)$$

where the matrix elements can be explicitly calculated as a function of the magnetization direction.  $\xi_d$  characterizes the strength of the SO coupling, and is taken to be 86 meV [20]. The spin-orbit coupling will cause a dependence of total energy on the spontaneous magnetization direction - the aforementioned magneto-crystalline anisotropy. The shape of the particle is transmitted to the magnetic anisotropy after many steps along the electron hopping paths. The last term in (1), is a local one-body operator describing the coupling of the spin and orbital degrees of freedom to an external magnetic field.

$$\mathcal{H}_{\text{Zeeman}} = -\mu_B \sum_{i\mu\mu's's'} \langle \mu s | \vec{L} + g_s \vec{S} | \mu' s' \rangle \vec{H}_{\text{ext}} c_{i\mu s}^\dagger c_{i\mu' s'} \quad (8)$$

The simplified mean-field Hamiltonian now appears as follows,

$$\begin{aligned} \mathcal{H}_{MF}(\vec{h}) &= \mathcal{H}_{\text{band}} + \mathcal{H}_{SO} + \mathcal{H}_{\text{Zeeman}} \\ &+ \frac{\vec{h} \cdot \vec{h}}{2J} (g_s \mu_B)^2 N_a - 2g_s \mu_B \vec{h} \sum_i S_{di} \end{aligned} \quad (9)$$

The self-consistent spin-splitting field  $\vec{h}^*$  will minimize the expectation value of the Hamiltonian, yielding the ground state energy,  $E(\vec{h}^*) = \langle \mathcal{H}_{MF}(\vec{h}^*) \rangle$ . By diagonalizing  $\mathcal{H}_{MF}$  we obtain a set of quasiparticle eigenenergies, which are occupied up to the Fermi level.

This simplified model of ferromagnetic nanoparticles has the obvious advantage of being able to treat larger clusters, possessing a much greater computational simplicity than first principles models. It will provide us with the generic properties of ferromagnetic nanoclusters, without having to resort to the much more costly spin density functional theory. In particular, the detailed properties of the electron hopping network will depend on atom position relaxations within the nanoparticle. We view the model outlined above having an appropriate level of detail to address properties for which these relaxations are unimportant.

In the experiment of Ref.1 the distances between two Cobalt atoms, which are registered to the Si substrate, are larger than bulk Cobalt, implying that the magnitude of the hopping parameters entering the tight-binding model should be smaller than the bulk values. In this paper we did not try to rescale the hopping parameters. However, since the crucial parameter that controls the magnetic properties of the nanoplatelets is likely to be  $J/W_d - W_d$  being the width of the  $d$ -band – the effect of a smaller  $W_d$ , could partly be mimicked by increasing the value of  $J$ , while keeping the hopping coefficients constant. This is one of the reasons of our interest in studying the  $J$  dependence of the magnetic properties.

### C. Perturbative analysis

A qualitative understanding of the system features can be achieved through the use of perturbation theory. In bulk ferromagnets, the SO interactions are relatively weak, allowing the use of second-order perturbation theory to estimate the energy shifts. If we completely turn off the SO interaction, the eigenstates of a single-particle Hamiltonian are rotationally invariant and of pure spin character. Turning on the SO interaction, the degeneracy is lifted and the new eigenfunctions are of mixed spin character. The complete quenching of the orbital angular momentum is counteracted by the SO interaction that when treated as a perturbation yields the second-order correction

$$\varepsilon_{SO} \equiv \varepsilon_{ns} - \varepsilon_{ns}^{(0)} = \frac{\xi_d^2}{4} \sum_{s', m \neq n} \frac{|\langle \psi_{ms'}^{(0)} | \vec{L} | \psi_{ns}^{(0)} \rangle \cdot \vec{\tau}_{ss'}|^2}{\varepsilon_{ns}^{(0)} - \varepsilon_{ms'}^{(0)}} \quad (10)$$

where the superscript (0) stands for the unperturbed single particle wavefunctions and energies,  $n$  is an eigenstate label,  $s$  a spin label with the magnetization orientation direction  $\hat{\Omega}$  chosen as the quantization axis, and  $\vec{\tau}$  is a vector containing the three Pauli matrices. The matrix elements are most easily evaluated by transforming  $\vec{\tau}$  to the orbital coordinate system. Unlike the infinite solid, where only states of the same  $\vec{k}$  that are typically separated by an energy of the order of the bandwidth  $W_d$  are coupled, a given state in a nanoparticle is coupled to many other orbitals by the spin-orbit interaction.

Simplifying Eq.(10) and averaging over the nine Co orbitals, we can evaluate the typical SO energy shift as

$$\varepsilon_{SO} = \frac{\xi_d^2}{W_d} \quad (11)$$

For Co,  $\xi_d = 86$  meV and  $W_d \sim 5$  eV, yielding a typical energy shift of 1.5 meV. This formula should hold for both bulk material and particles, provided there are no significant correlations between angular momentum matrix elements and quasiparticle energy differences. The anisotropy energy is to a good approximation given by a partially canceling sum of spin-orbit induced energy

shifts depending on magnetic orientation. Because of these cancellations, the anisotropy energy is in general much smaller than  $\varepsilon_{SO}$ . In a finite system there is always a perturbative coupling between quasiparticle states close in energy in Eq. (10), but the matrix elements are distributed among many states, meaning that typical energy shifts should be comparable to those in bulk. In general, the anisotropies of particles are larger than those of bulk because of the loss of symmetry at the surface which tends to reduce cancellations.

### III. NUMERICAL RESULTS

#### A. FCC lattice truncation

We create our nanoplatelets by simply truncating the FCC lattice into 2 ML thick equilateral triangles, and selecting their surface oriented in parallel to a given crystal plane. In addition to the experimentally produced clusters, which we identified as having a surface parallel to the (111) plane, we also examine clusters that result from choosing a truncation plane parallel to the (001) crystal surface. These choices yield two different structures with different symmetries and coordination numbers. The number of nearest neighbors for an atom in the interior of the particle is 8 for the (001) geometry, but 9 for the (111). This difference is reflected in the number of next nearest neighbors, which is 4 for the (001) and 3 for the (111) geometry. The configuration of next and nearest neighbors will determine the active hopping matrix elements parameterized by the Slater-Koster parameters in the term  $\mathcal{H}_{\text{Band}}$  in the Hamiltonian (2), i.e. the orbital motion of the electrons inside the nanoparticle.

Examples of structures resulting from choosing two different truncation planes are shown in Fig. 1. We note that the resulting (111) geometry has a higher degree of symmetry with a three-fold rotation axis running perpendicularly through the triangle surface and three mirror planes, whereas the (001) version only has a mirror symmetry across the vertical axis. These symmetries must all be preserved in the magnetic anisotropy energy landscape resulting from the particle. One additional symmetry will always be present in all anisotropy landscapes, irrespective of shape or size. Due to time-reversal invariance we will always have the inversion symmetry,

$$E(\theta, \varphi) = E(\pi - \theta, \pi + \varphi) \quad (12)$$

where  $\theta$  and  $\varphi$  are the spherical coordinates that define the magnetization direction,  $\hat{\Omega}$ . Throughout this article, we will fix our coordinate system as in Fig. 2, with the z-axis ( $\theta = 0$ ) perpendicular to the nanoplatelet surface and the y-axis ( $\theta = \pi/2, \varphi = \pi/2$ ) parallel to the surface and in one of the mirror symmetry planes of the cluster. In addition to the above described clusters have also examined one monolayer thick clusters, obtained by simply removing the top layer of a (111) cluster of a given size.

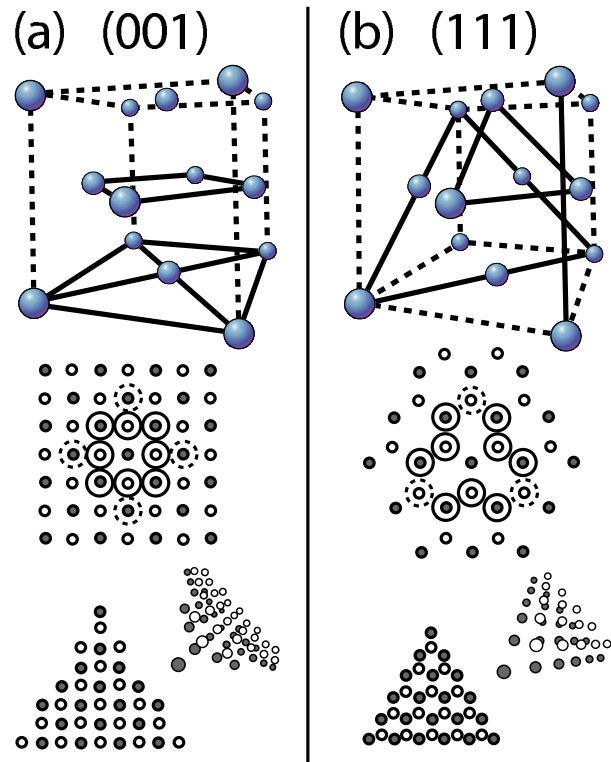


FIG. 1: The structure resulting from choosing two different planes of truncation for the 2 MLs of the nanoparticle. The left column (a) shows the effect of choosing the nanoplatelet surface parallel to the (001) FCC crystal plane and the right column (b) depicts the situation obtained by instead selecting the (111) FCC crystal plane. The top row shows the FCC unit cell with the nanoparticle atoms connected by solid lines. In second row there is a top view of the 2 MLs selected in the unit cells above. The dashed circles indicate the next nearest neighbors solid circles indicate the nearest neighbors of an atom in the interior of the nanoparticle. Finally, the bottom row shows the resulting nanoparticle (top view and in perspective).

#### B. Magnetic Moments

Fig. 3 shows the mean magnetic moment per atom for increasing cluster size with one curve for  $J = 1.0, 1.5$  and  $2.0$  eV. The increase in the mean moment with  $J$  occurs because the system more strongly favors the alignment of spins in the  $d$ -channel, and the spin-character of the eigenstates becomes more well defined. This behavior is associated with a redistribution of  $d$ -charge into the  $p$ - and  $s$ -channels. By altering the electronic configuration of the  $3d$  levels and increasing the number of singly occupied levels, the total energy is decreased. We will address this issue in more detail below.

The atomic mean magnetic moment curves level out above 100 atoms and we can extract the approximate values for the smallest of the experimentally produced nanoplatelets, i.e. the one consisting of roughly 225 atoms. The mean magnetic moments per atom are presented in table I. The 1 ML value corresponds to taking

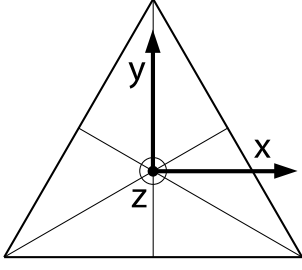


FIG. 2: We define our coordinate axis relative to the triangular nanoplatelet, with the z-axis perpendicular to the surface, and the y-axis parallel to the surface and in a mirror symmetry plane (unique in the case of (001)).

	2 ML (111)	2 ML (001)	1 ML (111)
$J = 1.0$ eV	$2.32\mu_B$	$2.44\mu_B$	$2.57\mu_B$
$J = 1.5$ eV	$2.87\mu_B$	$2.99\mu_B$	$3.99\mu_B$
$J = 2.0$ eV	$3.48\mu_B$	$3.84\mu_B$	$4.31\mu_B$

TABLE I: The mean magnetic moment per atom for the  $\sim 225$  atom clusters (the 1 ML cluster has 120 atoms)

the top layer off the 225 atom 2 ML (111) version, yielding a cluster consisting of 120 atoms.

We can compare these values with the experimentally observed value for the mean magnetic moment  $\mu = 2.1 \pm 0.2\mu_B$  [1]. Only the  $J = 1.0$  eV setting will produce a similar value. We nevertheless include larger values of  $J$  in the following calculations in order to address the physics underlying anisotropy energy trends. Both 2 ML clusters display similar behavior, but the 1 ML (111) cluster exhibits a slight relative enhancement of the mean magnetic moment. In the 2 ML clusters, a second monolayer induces cancellation effects, with a subsequent drop in the mean moment value. In general, the number of unbalanced spins increases with the surface to volume ratio of the nanoparticle. The difference between the 2 ML (001) clusters and the 2 ML (111) clusters can be attributed to the lower symmetry of the (001) cluster.

### C. Magnetic Anisotropy Landscapes

Magnetic anisotropy energy landscapes have been computed for the three geometries described in the previous subsection (1 and 2 ML (111) and 2 ML (001)) for increasingly larger cluster sizes, up to approximately 225 atoms.

The results of these calculations reveal two major types of anisotropy landscapes. First, we have the Quasi-Easy Plane (QEP) which consists of a discrete number of in-plane energy minima, corresponding to easy directions consistent with the symmetries of the particle. These minima are separated by very low energy barriers, thus forming a quasi-easy plane oriented in parallel with the

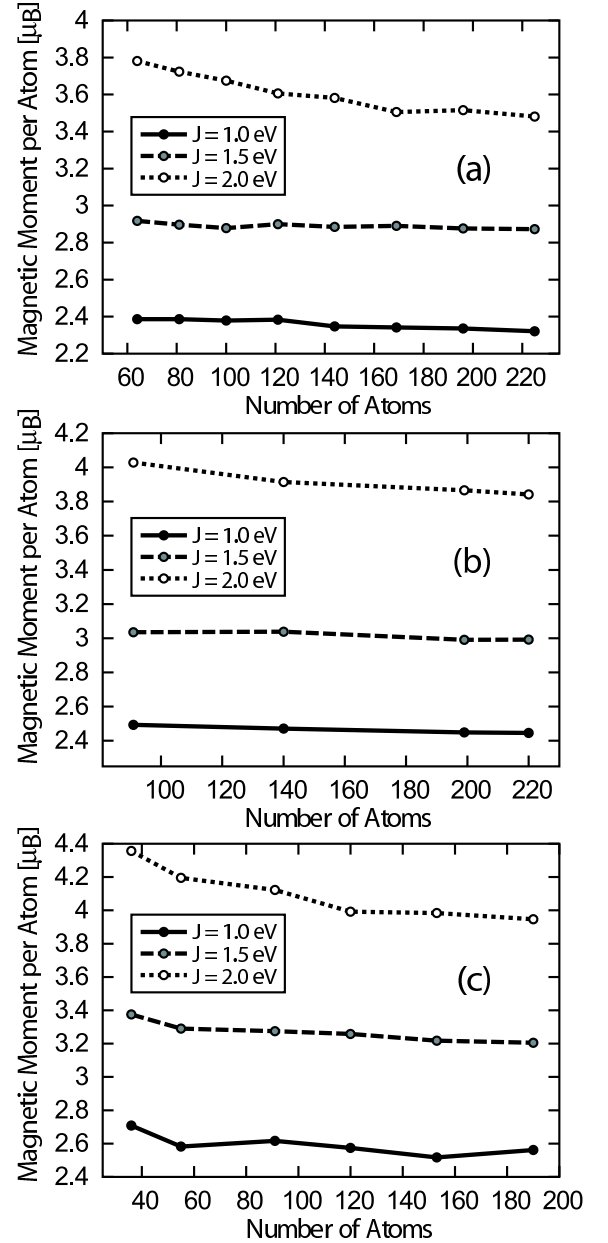


FIG. 3: The atomic mean magnetic moment as a function of cluster size for the different  $J$  and all geometries - (a) 2 ML (111), (b) 2 ML (001) and (c) 1 ML (111). The relatively elevated values of 1 ML (111) is associated with imbalance effects brought on by a larger surface area. The experimental mean magnetic moment is approximately  $2.1 \pm 0.2\mu_B$  [1], which is similar to the value obtained for 2 ML clusters and  $J = 1.0$  eV.

surface of the nanoplatelets. The second type of observed anisotropy landscape, corresponds to a bistable system with two easy directions oriented perpendicularly to the cluster surface, separated by a large blocking barrier.

We have explored the parameter space governing the resulting anisotropy landscape keeping track of three variables: the type of geometry, the size of the cluster ( $\lesssim 225$  atoms), and the value of the exchange coupling



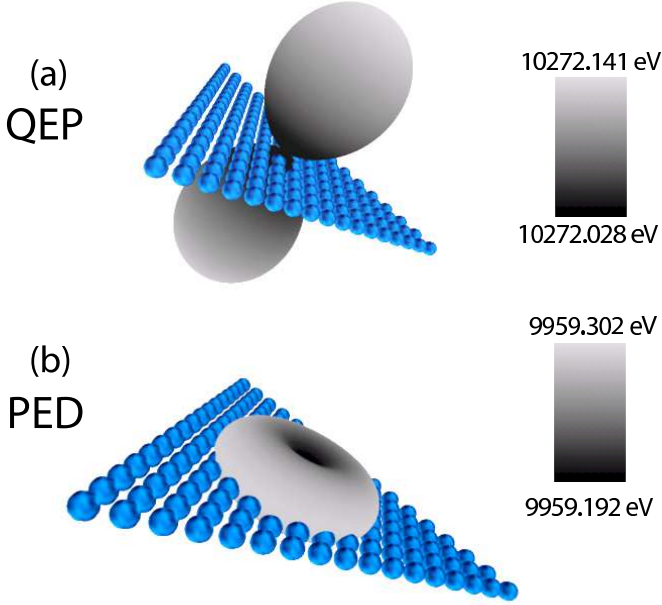


FIG. 4: The two typically observed anisotropy energy landscapes exemplified by 153 atoms of 1 ML (111). (a) shows the Quasi-Easy Plane (QEP) solution and (b) the landscape with Perpendicular Easy Directions (PED). These graphs show how the energy varies with the direction of the self-consistent spin splitting field on the unit sphere, and have been rescaled so that the minimum energy is located at the origin and the maximum at unity (see Eq. (13)-(15)). For clarity, the energy value has also been color coded and the individual atoms superimposed. The colorbars on the right show the grayscale interpolation between the maximum (top, white) and minimum (bottom, black) energy in eV.

strength ( $J = 1.0, 1.5$  and  $2.0$  eV). Qualitatively, we can separate our results into two size regimes - a small cluster regime consisting of 50 atoms and less, and a large cluster regime consisting of clusters that have more than 50 atoms.

In the large cluster regime ( $> 50$  atoms) all geometries exhibit quasi-easy planes for  $J = 1.0$  eV. In contrast, for  $J = 1.5$  and  $2.0$  eV all of these clusters produce landscapes with Perpendicular Easy Directions (PEDs). The two typical landscapes always take an approximate form exemplified in Fig. 4 by 153 atoms of 1 ML (111). In this figure, the energy landscape on the unit sphere has been renormalized according to the equations

$$x = \frac{E(\theta, \varphi) - E_{\min}}{E_{\max} - E_{\min}} \sin \theta \cos \varphi \quad (13)$$

$$y = \frac{E(\theta, \varphi) - E_{\min}}{E_{\max} - E_{\min}} \sin \theta \sin \varphi \quad (14)$$

$$z = \frac{E(\theta, \varphi) - E_{\min}}{E_{\max} - E_{\min}} \cos \theta \quad (15)$$

so that at any given point the distance from the origin corresponds to the energy value, with the minimum value

$N_a \leq 50$	2 ML (111)	2 ML (001)	1 ML (111)
$J = 1.0$ eV	QEP/PED	QEP	QEP
$J = 1.5$ eV	QEP/PED	QEP	PED
$J = 2.0$ eV	PED	PED	PED
$N_a > 50$	2 ML (111)	2 ML (001)	1 ML (111)
$J = 1.0$ eV	QEP	QEP	QEP
$J = 1.5$ eV	PED	PED	PED
$J = 2.0$ eV	PED	PED	PED

TABLE II: Qualitative behavior of the clusters with less than (top) and more than (bottom) 50 atoms.

located at the origin and a maximum value at a distance of unity.  $\theta$  and  $\varphi$  refer to the polar and azimuthal angle, respectively. In addition to the rescaling, the distance from the origin has been color coded for viewing convenience - the black minima that appear in these shapes correspond to the easy directions.

Turning to the more sensitive regime of small clusters ( $\leq 50$  atoms), the 1 ML (111) and the 2 ML (001) clusters display only QEPs for  $J = 1.0$  eV. For the same setting of  $J$  and 2 MLs of (111), we instead find a wide range of intermediate shapes between the QEP and PED landscapes. Most notably, the 2 ML (111) clusters are the only ones capable of producing a clear bistable system with PEDs for the original setting of  $J = 1.0$  eV. This behavior indicates that the 2 ML clusters generated in the (111) plane are more prone to forming a perpendicular bistable system than their (001) counterparts. The qualitative behavior of the anisotropy landscapes in the two different size regimes is summarized in table II. Note QEP/PED means that quasi-easy planes (QEP), perpendicular easy directions (PED) and intermediate shapes between these are observed in the small cluster regime. No qualitative change in any of the anisotropy landscapes can be observed for  $J > 2.0$  eV, indicating that we have already reached a saturation of the effect brought on by increasing the exchange.

Traces of the symmetries of the particle resulting from the chosen geometry are present in the associated anisotropy landscapes with a varying degree of visibility. The way in which the symmetry of the particle is reflected in the anisotropy landscape is most easily identified by considering the configuration of discrete minima in the quasi-easy plane landscapes (see Fig. 5). These figures show the local maxima/minima structure in the xy-plane that coincides with the surface of the nanoplatelets.

Group theoretical considerations for the FCC lattice geometry predict a six minima structure. Although we break the full FCC symmetry by selecting only a few monolayers, this six minima structure is still present in the (111) clusters, identifiable as the easy directions parallel to the symmetry lines of the equilateral triangle running from the corner to the midpoint of the opposing line. In the (001) case the symmetry is even more badly broken and there are only two remaining minima corresponding

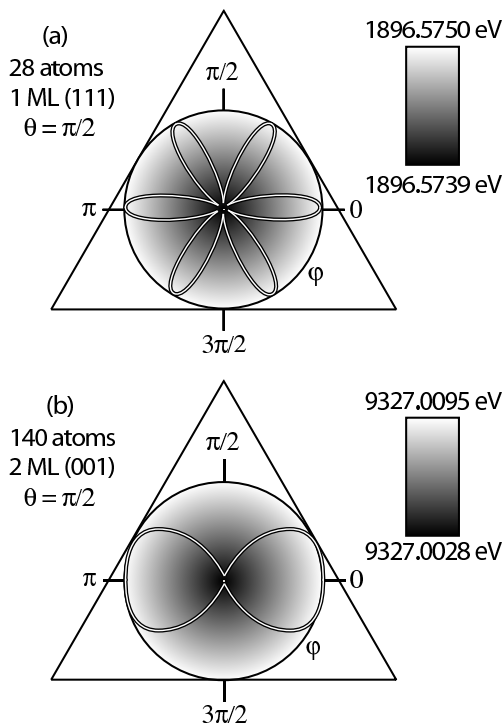


FIG. 5: Examples of the discrete minima structure in the quasi-easy planes for (a) 1 and 2 ML (111) and (b) 2 ML (001). The black and white lines in the circle trace out the section of the MAE landscape in the xy-plane parallel with the cluster surface ( $\theta = \pi$ ), renormalized so that the origin corresponds to the energy minimum and the radius of the circle to the (local) maximum (see Eq. (13)-(15)). The grayscale background in the circle shows how the energy varies with distance from the origin, with minimum energy at the origin (black) and maximum at the circle radius (white). The numerical values of the max. and min. are given at the top and bottom of the colorbar on the right. The six- and two-fold minima are consistent with the symmetries of the particle. Note that the (111) in-plane barrier is significantly smaller than that of (001).

	2 ML (111)	2 ML (001)	1 ML (111)
$J = 1.0$ eV	-0.10 meV	-0.69 meV	-1.02 meV
$J = 1.5$ eV	0.58 meV	0.49 meV	0.74 meV
$J = 2.0$ eV	0.02 meV	0.17 meV	0.45 meV

TABLE III: The anisotropy energies per atom corresponding to the  $\sim 225$  atom nanoplatelets.

to in-plane easy directions parallel to the mirror symmetry line, running vertically through the center of the particle. Similar symmetry effects can be seen to a lesser extent in the perpendicular easy direction landscapes, either as a hint of a hexagonal shape replacing the circular rim of the torus in the case of the (111), or as a weakly oval toroid in the (001) case.

## D. Anisotropy Energies

Fig. 6 shows how the anisotropy energy per atom varies with the number of atoms. As before, each diagram represents a different geometry, and each curve represents a specific value of  $J$ . The anisotropy energy is defined with a sign as the in-plane direction energy minus the perpendicular direction energy, so that a negative value corresponds to QEPs and a positive to PEDs. The horizontal lines mark the experimental ( $\approx 0.4$  meV) and bulk ( $\approx 0.045$  meV) value. Table III displays the anisotropy energy per atom for the approximate sizes corresponding to the smaller of the two dimensionally quantized clusters grown (225 atoms).

We expect fluctuations in the anisotropy energy to be large for the smaller clusters, where our mean-field treatment is less accurate. It is obvious however, that the fluctuations are larger for the (111) in comparison to (001). Some fluctuations can be caused by the failure of mean field theory, but in the 2 ML (111) case the fluctuations persist even for relatively large clusters between 50-100 atoms. The fluctuations in this region for the 2 ML (111)  $J = 1.5$  eV curve, can be attributed to the phenomenon of weakly avoided level-crossings [2], that can occur as the model parameter space is varied - particularly for smaller clusters.

We note that the ordering of the absolute magnitude of the energies with respect to  $J$ , is not the same for the different geometries. For 2 ML (001) and 1 ML (111) the anisotropy energy magnitude follows a generally decreasing trend with increasing  $J$ . In the case of 2 ML (111) the  $J = 1.5$  eV curve starts to climb rather steeply and overtakes the  $J = 1.0$  eV magnitude around 100 atoms. For a given cluster size, perturbation theory predicts that the magnitude of the anisotropy energy will initially increase as a function of small  $J$ , and decrease asymptotically for large  $J$ . The turning point of the anisotropy magnitude as a function of the exchange strength will be different for the different geometries, which explains the different ordering of the magnitudes in figure 6. In figure 7 we have mapped out the exchange strength versus anisotropy energy in order clarify this difference between the (001) and the (111) geometries.

## IV. DEPENDENCE OF QUASIPARTICLE SPECTRUM ON EXCHANGE COUPLING

In order to shed light on the overall magnetic behavior of the nanoplatelets described above, in this section we study the properties of the underlying quasiparticles and how they depend on the exchange coupling  $J$ .

### A. Quasi-particle energy levels and eigenstates

We start by looking at the “band structure” for three different values of  $J$ . In Fig. 8 the quasiparticle energies



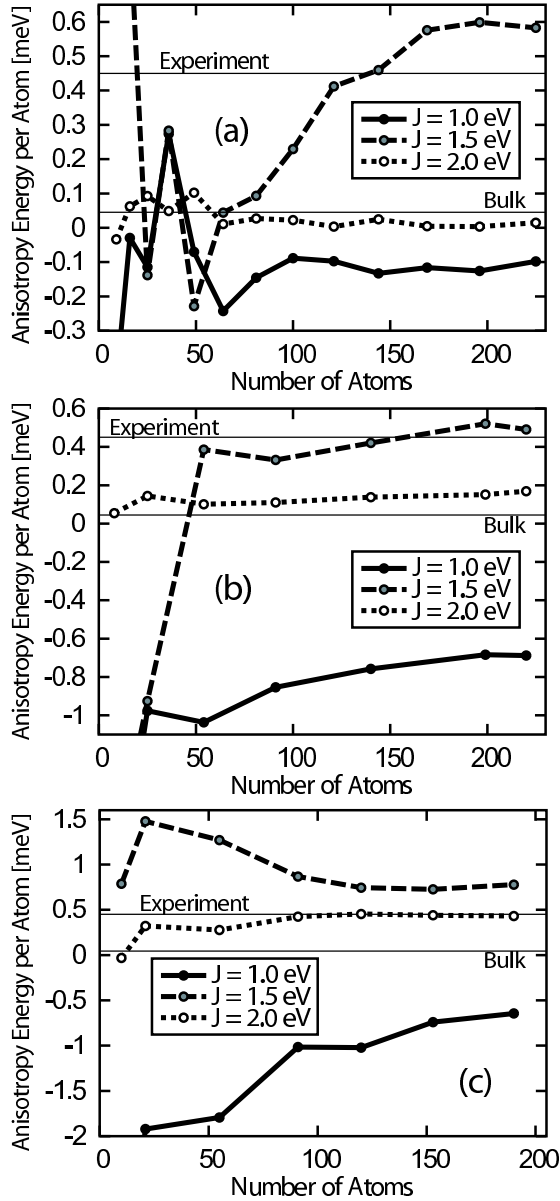


FIG. 6: The anisotropy energy per atom as a function of cluster size for different  $J$  and the three different geometries - (a) 2 ML (111), (b) 2 ML (001) and (c) 1 ML (111). Each curve represents a different value of the exchange coupling. A negative sign indicates QEPs and a positive PEDs. Some fluctuations are to be expected, particularly for the smallest clusters, where the mean-field treatment is not so accurate. 1 ML (111) displays a generally higher anisotropy energy due to larger unbalanced spin populations.

are plotted as a function of eigenvalue index up to Fermi level for 225 atoms of 2 ML (111). The behavior for the three systems considered so far— 2 ML (111), 2 ML (001) and 1 ML (111)— is qualitatively similar. The spectrum is characterized by a low-energy part that increases linearly with the eigenvalue index and extends up to roughly mid spectrum where there is a shoulder that becomes more pronounced with increasing  $J$ . As we show below, the

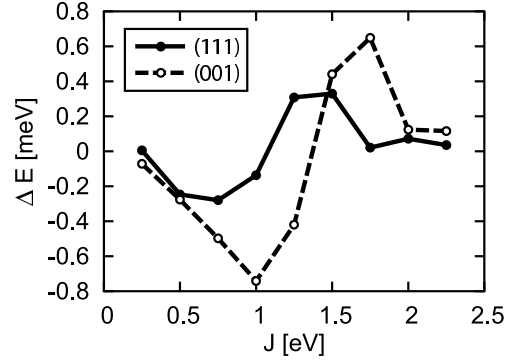


FIG. 7: The anisotropy energy as a function of  $J$  for  $\sim 140$  atom clusters of 2 ML (001) and (111) reveals a curve that roughly agrees with what one might expect from perturbation theory. The transition from QEP to PED (minus to plus) occurs for smaller  $J$  in the case of the (111) cluster, indicating a bias toward PED for this geometry.

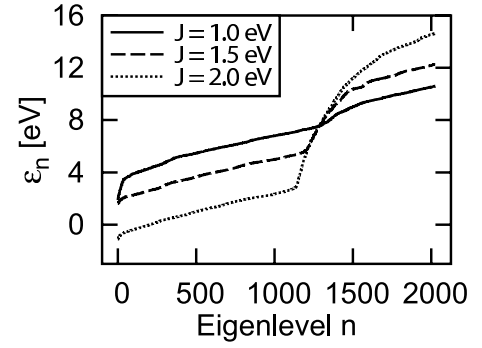


FIG. 8: The eigenenergies of all occupied levels for 225 atoms of 2 ML (111). The spin-aligned region (below the curve discontinuity) of pure  $d$ -character lowers the total energy via the exchange term. This is at the cost of a rise in the total energy due to the higher, mixed states. The resulting total energy is minimized by balancing the energy cost and gain associated with these two regions. All geometries display a similar linear low energy region and a discontinuous mid-spectrum leap.

low-energy states are majority-spin states of predominant  $d$ -character. From the figure we can see that increasing  $J$  simply causes a rigid down-shift of this part of the spectrum, while the width of the spectrum about the shoulder increases considerably.

In order to determine the orbital mixing of the eigenlevels, we can project out the  $s, p$  and  $d$  characters using the associated projection operator.

$$P_\ell = \sum_i \sum_s \sum_{\mu_\ell} |i, \mu_\ell, s\rangle \langle i, \mu_\ell, s| \quad (16)$$

where  $\ell = s, p, d$  and the projection operators fulfill the sum rule

$$\sum P_\ell = P_s + P_p + P_d = 1 \quad (17)$$

The result of this operation is shown in figure 9 for 225 atoms of 2 ML (111), where the three orbital channels

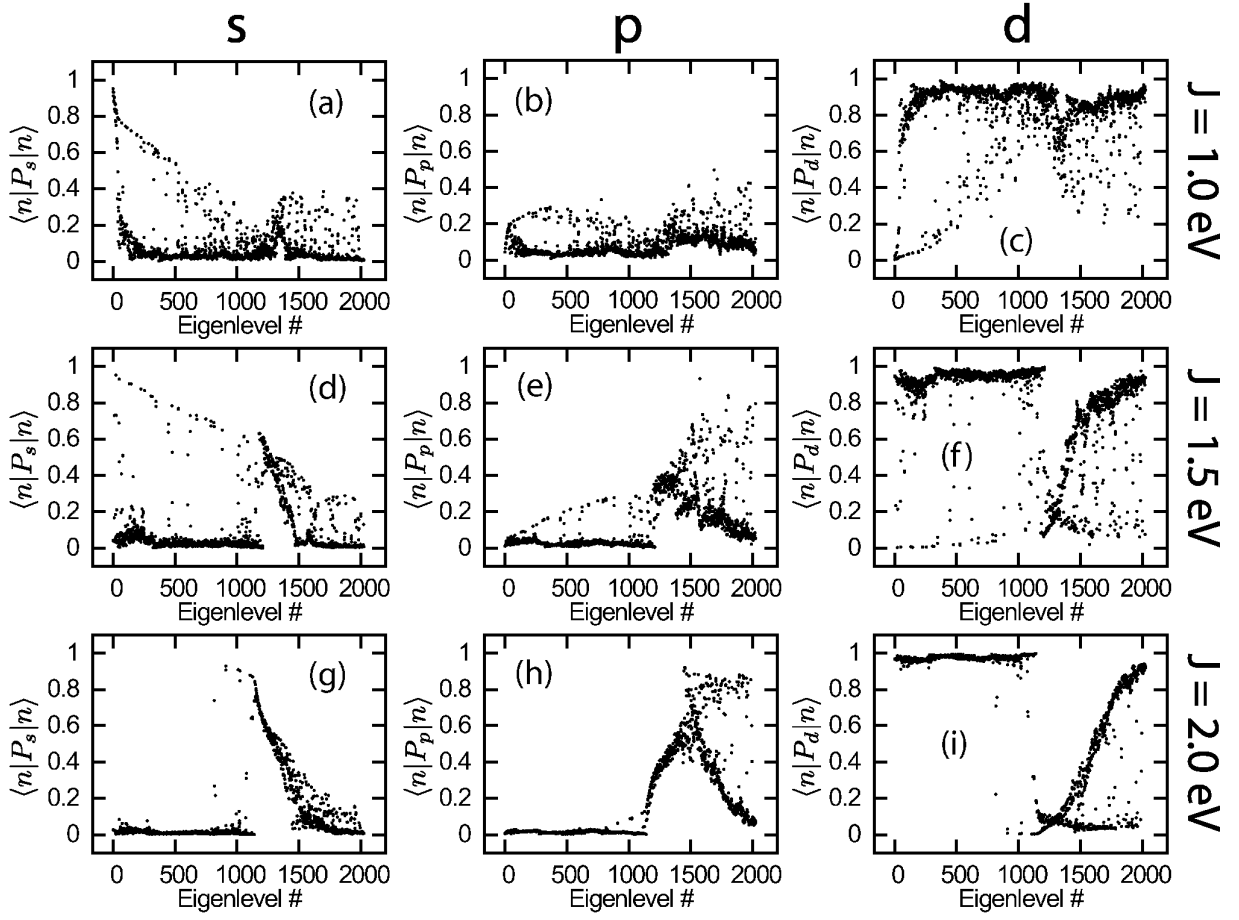


FIG. 9: The orbital character of the occupied eigenlevels for a 225 atom 2 ML (111) cluster. Each column shows the respective  $\ell$ -channel obtained by applying the associated projection operator as defined in Eq. (16), and each row refers to a different value of the exchange coupling. Increasing  $J$  prompts the formation of a virtually pure  $d$ -character region covering the lower half of the eigenspectrum, and the levels with high  $s$ - and  $p$ -level mixing are focused on the upper half of the spectrum. Note that the high  $d$ -mixing returns just below the Fermi surface. The other geometries display a qualitatively similar evolution of the orbital character mixing pattern with increasing  $J$ .

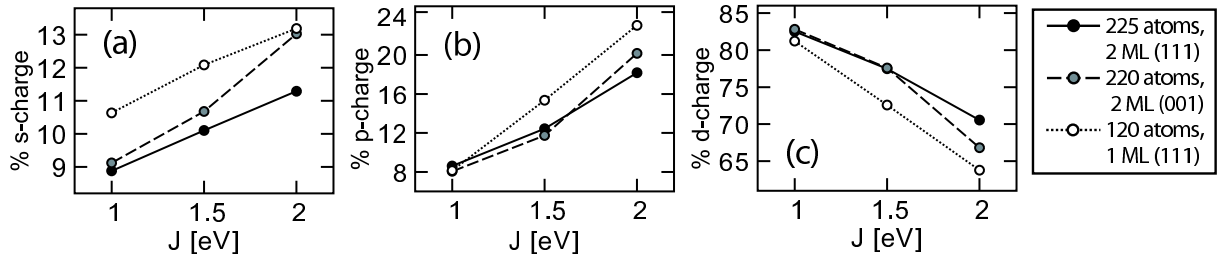


FIG. 10: The total percentage of  $\ell$ -charge for the representative clusters. Orbital character changes such that the  $s$ - and  $p$ -channels become more populated at the expense of the  $d$ -channel with increasing  $J$ .

have been separated. At  $J = 1.0$  eV, the mixing is fairly homogeneous over the range of eigenlevels, with an overshadowing total percentage of  $d$ -character, as is expected for Co. Remarkably, as  $J$  is increased, redistribution of charge results in a configuration where roughly all levels in the lower half of the spectrum obtain a pure  $d$ -character. Above this eigenlevel, two distinct lines of mixing can be observed. The first one skims the bottom

of the  $d$ -channel and represents levels with a very low  $d$ -character mixing. Secondly, there is a line of mixing representing the other half of the eigenlevels in the upper region, telling us that they obtain an increasing mixture of  $d$  with the eigenenergy, such that at the Fermi surface, the character is almost 100%  $d$  again.

Increasing  $J$ , the  $s$ -charge vacates the lower region, making way for the  $d$ -charge and lodges mostly in a nar-

row region above the pure  $d$ -levels. The  $p$ -charge exhibits a similar evolution pattern, but ends up with a maximum in the center of the upper half of the spectrum. The other geometries - 1 ML (111) and 2 ML (001) - display a qualitatively similar behavior when projecting out the different channels.

Fig. 10 shows the total percentages of  $\ell$ -charge in the nanoparticle. By inspection, we see that the above described segregation of orbital character of the eigenlevels with the energy, is associated with a general funneling of  $d$ -charge mainly into the more energetic  $p$ -levels, but we also find a smaller percentage going into the  $s$ -channel. Comparing the 2 ML (001) and 2 ML (111) curves, we see that the redistribution when  $J$  is increased is more pronounced for the (001) symmetry.

### B. Quasi-particle spin

We next discuss the  $J$ -dependence of the spin character of the quasi-particle states. It is useful to define our axis relative to the triangular nanoplatelet as in figure 2, with the  $z$ -axis perpendicular to the surface, and the  $y$ -axis parallel to the nanoplatelet surface and one of the triangles symmetry lines. In Fig. 11 we plot the quasi-particle expectation values  $\langle n|S_i|n\rangle$  of the component of the spin operator  $S_i$  in the direction of the magnetization, that is, along the  $y$ -axis for  $J = 1.0$  eV and along the  $z$ -axis for  $J = 1.5$  eV and  $2.0$  eV. We have verified that the expectation value of the component of the spin operator in other directions is negligible. The numerical results shown here are for the 225 atom 2 ML (111) system. The other two geometries considered display a very similar trend. As anticipated in the previous section, when we discussed the energy spectrum in Fig. 8, for  $J = 1.0$  eV the low-energy states up to the energy shoulder correspond to (predominant) majority-spin states; above the shoulder, at the top of the majority-spin band, the minority-spin band starts. For  $J = 1.0$  eV there are however several states whose spin is not well-defined. When  $J$  increases to  $1.5$  and  $2.0$  eV, most of the states acquire a well-defined spin character and there is a conversion of minority-spin states into majority spins leading to an increase of the net spin magnetic moment (see Fig. 3). As we can see in Fig. 9, the change in spin character is also accompanied by a change in orbital character, in which the  $d$ -states are redistributed into the  $p$ - and  $s$ -channels. Nevertheless the Fermi levels still lies among states of predominant  $d$ -character. For  $J = 1.5$  and  $2.0$  eV the majority- and minority-spin bands overlap. The shoulder seen in Fig. 8 occurs at the bottom of the minority-spin band. For  $J = 2.0$  eV the majority-spin density of states at the Fermi level is not zero but much smaller than the minority-spin density of states.

### C. Quasi-particle anisotropy energies

The quasi-particle anisotropies are obtained by taking the difference between the eigenenergies of level  $i$  in the hard and easy direction. Table IV displays the standard deviations of the distributions for the three different clusters. Typically, the width of the distribution is between one to two order of magnitude larger than the mean value, indicating that the resulting sum of anisotropies has large cancellations and that individual levels may shift the value of the total anisotropy.

In Fig. 12 we plot the cumulative sum of individual quasi-particle anisotropy energies, i.e.

$$\mathcal{C}(\mathcal{N}_e) = \sum_{n=1}^{\mathcal{N}_e} [\varepsilon_n(\hat{y}) - \varepsilon_n(\hat{z})], \quad (18)$$

where we sum over an increasing total number of occupied quasiparticle states  $\mathcal{N}_e$ , and display the result as a function of the “band filling”, that is,  $\mathcal{N}_e$  divided by the number of atoms  $\mathcal{N}_A$ . The vertical line at  $\mathcal{N}_e/\mathcal{N}_A = 9$  corresponds to the cobalt band filling. The result reveals large and rapidly varying fluctuations of  $\mathcal{C}(\mathcal{N}_e)$  as a function of the band filling. This supports the idea that the total anisotropy energy is given to a good approximation by a partially canceling sum of quasiparticle anisotropies, and that only a fraction of states below the Fermi level is responsible for the overall anisotropy-energy characteristics of the system [2]. For the particular case of the 2 ML (111) shown in the figure, we can see that the cumulative density at cobalt band filling as a function of  $J$  experiences a sharp maximum in the vicinity of  $J = 1.5$  eV, which accounts for the behavior of the total anisotropy energy displayed in Fig. 6. Similar sharp patterns are present in the cumulative sum for clusters resulting from the other geometries.

Fig. 13 shows the contribution to the total anisotropy energy (with sign) coming from each  $\ell$ -channel for the 2 ML geometries. This orbital character filtering of the single-quasiparticle levels has been calculated using the equation

$$\mathcal{A}_\ell \equiv \sum_{n=1}^N [\langle n(\hat{x}) | P_\ell | n(\hat{x}) \rangle \varepsilon_n(\hat{x}) - \langle n(\hat{z}) | P_\ell | n(\hat{z}) \rangle \varepsilon_n(\hat{z})] \quad (19)$$

where  $\varepsilon_n(\hat{y})$  &  $\varepsilon_n(\hat{z})$  are the single particle eigenenergies for eigenstates  $|n(\hat{y})\rangle$  &  $|n(\hat{z})\rangle$ , corresponding to the solutions with the field constant  $\vec{h}$  oriented in parallel to the  $y$  and  $z$ -axis respectively (see figure 2). In this way, we obtain a measure of the total contribution to the anisotropy energy coming from the electrons of orbital character  $\ell$ .

From Fig. 13 we can see that in general the major contribution to the anisotropy energy comes from states of  $d$ -character, which tend to favor perpendicular anisotropy (note however that for small clusters,  $d$ -states can have in plane anisotropy). States of  $s$  character contribute little except for very small clusters. States of  $p$ -character

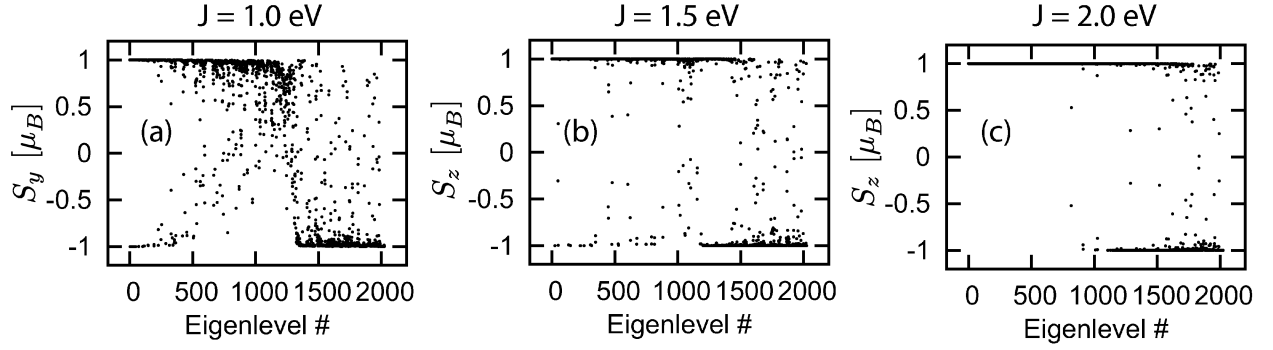


FIG. 11: The single-particle expectation value of the spin component along the easy axis (the direction of the nanoparticle magnetization). The spin character of the quasi-particle states becomes more well defined with increasing  $J$ . These results are for a 225 atom 2 ML (111) nanoplatelet. The other geometries display very similar evolution patterns with increasing  $J$ .

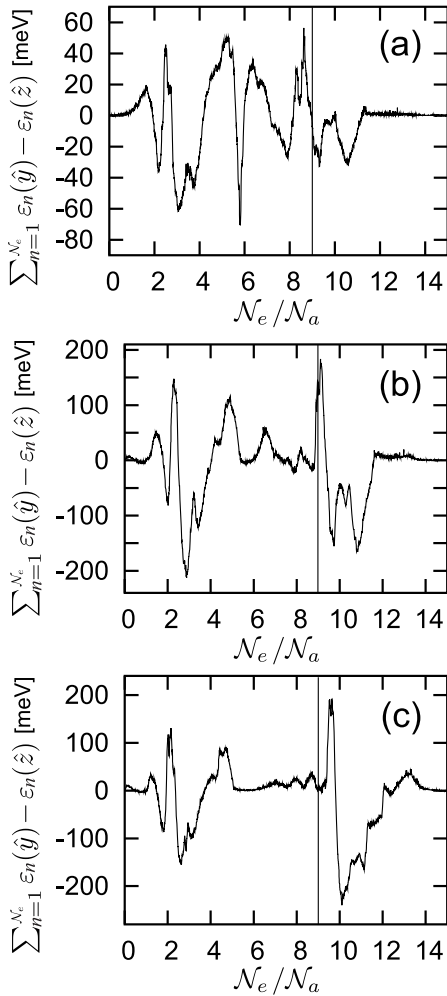


FIG. 12: Plot of the cumulative sum of single quasiparticle anisotropies (see Eq. 18) for 225 atoms of 2 ML (111) as a function of the “band filling”  $N_e/N_A$ , where  $N_e$  is the total number of occupied quasiparticle states and  $N_A$  is the number of atoms. The vertical lines mark the band filling for cobalt. The three panels refer to: (a)  $J = 1.0$  eV, (b)  $J = 1.5$  eV, and (c)  $J = 2.0$  eV respectively.

<i>System</i>	<i>J</i> [eV]	<i>Type</i>	$\sigma$ [meV]
225 atoms of 2 ML (111)	1.0	QEP	1.31
	1.5	PED	2.47
	2.0	PED	2.07
220 atoms of 2 ML (001)	1.0	QEP	2.61
	1.5	PED	1.93
	2.0	PED	1.70
120 atoms of 1 ML (111)	1.0	QEP	5.35
	1.5	PED	4.52
	2.0	PED	4.11

TABLE IV: Standard deviations for the distributions of single-level anisotropies as a function of increasing  $J$ .

mostly favor in-plane anisotropy and their relative contribution can be non-negligible. This trend is consistent with the fact that, as shown in Fig. 9, a few eigenstates around the Fermi level have strong  $p$  character when  $J \geq 1.5$  eV, but the anisotropy is still dominated by the most numerous  $d$ -character states.

#### D. Orbital contribution to the magnetic moment

Finally, we consider the  $J$ -dependence of the quasi-particle orbital moments, defined as the expectation value of the orbital angular momentum  $L$  with respect to the quasi-particle states  $|n\rangle$ . The matrix elements contain the normal local part of the orbital angular momentum, but also the non-local part originating from delocalized electrons under the influence of the spin-splitting field [28].

In the absence of SO interactions the orbital moment is quenched. When SO is present the orbital moments are non-zero and are believed to play a crucial role in the magnetic properties of magnetic nanostructures. For our magnetic nanoplatelets we find that: (i) the orbital moment is larger than the bulk value and contributes significantly to the total magnetic moment of the system;

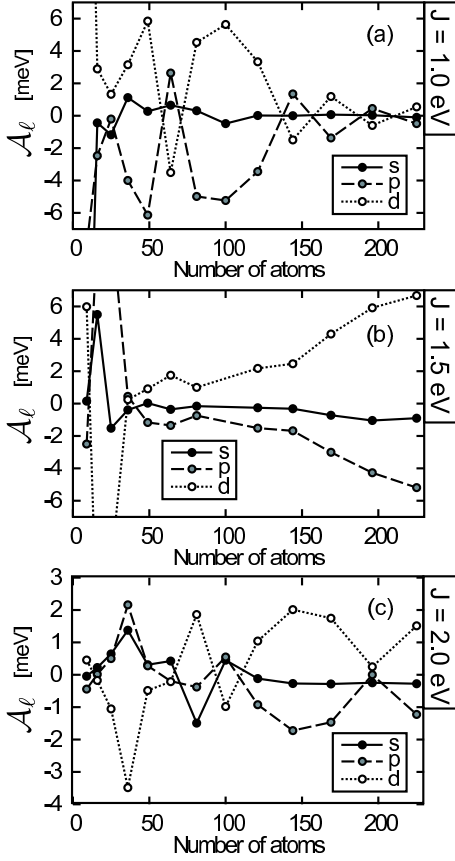


FIG. 13: The contribution to the anisotropy from each  $\ell$ -channel as a function of cluster size for the 2 ML (111) geometry.

(ii) the orbital moment is strongly anisotropic and its direction essentially coincides with the direction of the spin moment; (iii) its magnitude decreases as a function of  $J$ .

We are interested in the distribution of quasiparticle orbital contributions to the magnetic moment coming from all occupied eigenlevels computed when the spin-splitting field is chosen in the direction of the self-consistent solution. We compute expectation values in these states of the out-of-plane component  $L_z$  and the in-plane-component  $L_y$ . Note that for  $J = 1.0$  eV, when the magnetization is in the  $xy$ -plane, the  $y$ -axis corresponds to one of the discrete minima for the total energy (see Figs. 5 and 2) and we choose this direction for the self-consistent field.

For the quasi-in-plane  $J = 1.0$  eV solution, we find that there are sizable distributions in both  $y$  and  $z$  directions. Note that the  $x$ -component (not shown here) is negligibly small ( $< 10^{-10}$ ). Looking closely at the features of these distributions by means of Tab.V, we can see that the width of  $z$ -component is seven times wider than the  $y$ -component. However, the  $z$ -component is very symmetric around zero. Therefore the resulting average value is small  $\langle L_y \rangle \approx 0.007\mu_B$ . In contrast, the distri-

<i>System</i>	<i>J</i> [eV]	$\overline{\langle L_z \rangle}$	$\overline{\langle L_y \rangle}$	$\sigma_z$	$\sigma_y$
225 atoms of 2 ML (111)	1.0	-0.007	0.20	0.76	0.11
	1.5	0.18	-0.006	1.53	0.05
	2.0	0.08	-0.002	1.94	0.06
220 atoms of 2 ML (001)	1.0	0.003	0.25	0.24	0.13
	1.5	0.26	0.001	0.29	0.05
	2.0	0.09	$< 10^{-5}$	0.28	0.05
120 atoms of 1 ML (111)	1.0	-0.007	0.27	0.98	0.16
	1.5	0.09	-0.003	2.15	0.07
	2.0	0.04	-0.001	2.78	0.08

TABLE V: Statistics for the orbital matrix elements in units of  $\mu_B$ . Column 3 & 4 display the atomic mean orbital moment and the last two columns the standard deviation for the distribution of all eigenlevels. Large contributions to the matrix elements come only from the components along the easy-axis.

bution of the  $y$ -component is skewed around zero and its average is not small,  $\langle L_z \rangle = 0.20\mu_B$ . This value corresponds to an orbital moment =  $0.20\mu_B$ , larger than the cobalt bulk orbital moment  $0.14\mu_B$  per atom[29]. As  $J$  is increased to 1.5 eV, the magnetization direction switches from in-plane to out-of-plane. The distribution of the  $z$ -component widens whereas the  $y$ -component narrows. Furthermore, it is now the average orbital moment in the  $z$ -direction that is the dominant one ( $\langle L_z \rangle = 0.18\mu_B \gg \langle L_y \rangle = 0.006\mu_B$ ), although slightly smaller than the  $y$ -contribution of the  $J = 1.0$  eV case. When  $J$  is further increased to 2 eV, both  $\langle L_z \rangle$  and  $\langle L_y \rangle = 0.006\mu_B$  decrease. and become even smaller than the bulk value. The behavior for the the other two types of clusters is qualitatively similar.

Since the the orbital magnetic moment is strongly anisotropic and it is large when the total magnetic anisotropy is large, we can try to connect these two quantities. We follow Bruno's perturbative argument and we write [27]

$$E_{\text{ani}} = E(\hat{z}) - E(\hat{y}) = -\frac{1}{2} \frac{\xi(J)}{2\mu_B} (m_L^z - m_L^y), \quad (20)$$

where  $m_L^{z,y} = \mu_B \overline{\langle L_{z,y} \rangle}$ . For ferromagnetic transition-metal monolayers, this relationship is approximately satisfied when  $\xi \approx \xi_{\text{SO}}$  [27]. In our case the  $\xi$  is not directly related to  $\xi_{\text{SO}}$ ; it is smaller and depends weakly on  $J$ . Notice however that  $\xi(J)$  is positive and Eq. 20 captures the connection between the anisotropic character of the orbital moment and the sign of the anisotropy energy as a function of  $J$ .

## V. DISCUSSION

We have undertaken a theoretical study of magnetic anisotropy in small magnetic nanoparticles that is motivated in part by an experimental study of 2 ML thick Co

nanoplatelets grown by M.H. Pan et al [1]. Our study is based on a tight-binding model with short range exchange and atomic SO-interactions. Experimentally, the clusters are found to possess very high anisotropy energy per atom, approximately one order of magnitude larger than bulk value, with perpendicular easy directions (PED).

In addition to the experimental clusters, identified as having an FCC structure truncated in parallel to the (111) crystal plane and a modified lattice constant approximately equal to that of Si, we have studied the clusters resulting from instead choosing the plane of truncation in parallel to the (001) crystal plane. We found that the clusters with (111) geometry are more prone to forming magnetic anisotropy energy landscapes with perpendicular easy directions, an effect that can be traced to the difference in coordination number between the (111) and (001) geometries.

In our study the model parameter that influences the shape of the anisotropy landscape the most is found to be the intra-atomic  $d$ -electron exchange coupling strength,  $J$ . When  $J$  is set close to a value which reproduce the experimentally observed mean magnetic moment, all truncation schemes result in quasi-easy planes (QEP) for clusters larger than 50 atoms. For clusters smaller than this, only the 2 ML (111) geometry is capable of producing a clear bistable system, indicating a bias to PEDs for this symmetry. As  $J$  is increased to 1.5 eV and 2.0 eV all three geometries display PEDs, and the anisotropy energy per atom tends to decrease as the exchange is increased above the PED threshold value, identified as 1.5 eV. For  $J = 1.5$  eV and 2 ML of (111) we find both PEDs and a very high MAE per atom, in accordance with the experimental findings. Values of  $J > 1.5$  eV were considered here to investigate trends of the magnetic properties in the asymptotic regime of large exchange coupling, albeit they should not be regarded as physical.

Our simple model is able to produce the approximate scale of the MAE in very anisotropically shaped nanoparticles, to provide a sense of its dependence on electronic structure details, and an indication of its complex dependence on band-filling, exchange interactions strength, and other electronic structure parameters. Moreover, the model shows that the orbital magnetic moment is strongly anisotropic with a magnitude greater than bulk, and its behavior as a function of the model parameters reflects the behavior of the MAE. Nevertheless, when the phenomenological exchange constant of the model is chosen to reproduce the magnitude of the magnetization per atom, the anisotropy is underestimated and the sense of the anisotropy does not agree with the experiment of Ref. 1. Among the effects which we have neglected that could account for this discrepancy, two obvious possibilities are lattice-matching strains in the nanoparticle and

hybridization between nanoparticle substrate. In our calculations we have simply truncated the Co FCC structure with the normal Co lattice constant and used bulk values for the tight-binding model hopping parameters. The Co nanoparticles that motivated this study are in all likelihood registered epitaxially to the substrate, stretching the inter-atom distances in the platelet plain and perhaps reducing the inter-atom distance between the two planes. These altered atom-atom distances will alter the hopping parameters in a way that is likely described at least approximately by bulk scaling properties[30]. This additional anisotropy should likely be mainly uniaxial and could easily change the sense of the MAE. Hybridization with the substrate, corrugation of the surface, and inter-cluster magnetic dipole interaction are all sources of MAE neglected in our model. However, experimental results indicate that the effect of hybridization with Si is strongly diminished by introducing the 0.5 ML Al spacer layer. In addition, it can be seen that the effect of corrugation of the surface is minimal, by direct inspection of the STM-extracted Co cluster height curve. As long as the inter-cluster distance is sufficiently large (which it appears to be), we can most likely neglect the inter-cluster magnetic dipole interaction.

Our calculations suggest an alternative surface-physics based strategy for creating strongly anisotropic magnetic nanoparticles, namely the growth of Co clusters on a (001) Si surface covered with 0.5 ML of Al. To the best of our knowledge, such an attempt has not yet been made. Recent results [31] indicate that the 0.5 ML of Al will form dimers oriented parallel to the dimer ridges formed by the Si. Of course, the Si (001) surface is not homogeneous, but consists of domains of oriented dimer ridges, highly dependent on the annealing process. By tuning the Al deposition rate, it should be possible to obtain a substrate surface that is suitable for the growth of Co squares or rectangles. If this Co structure turns out to form a 2 ML (001) cluster, then that would result in a system with an anisotropy energy higher than the one for nanoplatelets grown on a (111) surface.

## VI. ACKNOWLEDGMENTS

We would like to thank Chih-Kang Shih for interesting discussions and Aleksander Cehovin for all his help with the computer codes. This work was supported in part by the Swedish Research Council under Grant No:621-2001-2357 and by the Faculty of Natural Science of Kalmar University. AHM acknowledges support from the Welch Foundation and from the NSF under grant DMR-0115947.

---

[1] M.-H. Pan, H. Liu, J.-Z. Wang, J.-F. Jia, Q.-K. Xue, J.-L. Li, S. Qin, U. M. Mirsaidov, X.-R. Wang, J. T. Marker,

et al., Nano Lett. **5**, 87 (2005).



- [2] A. Cehovin, C. M. Canali, and A. H. MacDonald, Phys. Rev. B **66**, 094430 (2002).
- [3] F. J. Himpsel, J. E. Ortega, G. J. Mankey, and R. F. Wills, Adv. Phys. **47**, 511 (1998).
- [4] R. Skomski, J. Phys.: Condens. Matter **15**, 841 (2003).
- [5] S. Ohnishi, A. Freeman, and M. Weinert, Phys. Rev. B **28**, 6741 (1983).
- [6] S. Blügel, B. Drittler, R. Zeller, and P. Dederichs, J. Appl. Phys. A **49**, 547 (1989).
- [7] S. Blügel and B. Drittler, Europhys. Lett. **9**, 597 (1989).
- [8] I. M. L. Billas, A. Châtelain, and W. A. de Heer, Science **265**, 1682 (1994).
- [9] I. M. L. Billas, A. Châtelain, and W. A. D. Heer, J. Magn. Mater. **168**, 64 (1997).
- [10] S. E. Apsel, J. W. Emmert, J. Deng, and L. A. Bloomfield, Phys. Rev. Lett. **76**, 1441 (1996).
- [11] S. Rusponi, T. Cren, N. Weiss, M. Epple, P. Bulushek, L. Claude, and H. Brune, Nature Materials **2**, 546 (2003).
- [12] P. Gambarella, A. Dallmeyer, K. Maiti, M. C. Malagoli, W. E. and K. Kern, and C. Carbone, Nature **416**, 301 (2002).
- [13] J. Bansmann, S. H. Baker, C. Binns, J. A. Blackman, J. P. Bucher, J. Dorantes-Dávila, V. Dupuis, L. Favre, D. Kechrakos, A. Kleibert, et al., Surf. Sci. Rep. **56**, 189 (2005).
- [14] L. Néel, J. Phys. Radium **15**, 225 (1954).
- [15] E. C. Stoner and E. P. Wohlfart, Phil. Trans. Phil. Roy. Soc. (London) **240**, 599 (1948).
- [16] M. Jamet, W. Wernsdorfer, C. Thirion, D. Mailly, V. Dupuis, P. Mélinon, and A. Péres, Phys. Rev. Lett. **86**, 4676 (2001).
- [17] P. Gambarella, S. Rusponi, M. Veronese, S. S. Dhesi, C. Grazioli, A. Dallmeyer, I. Cabria, R. Zeller, P. H. Dederichs, K. Kern, et al., Science **300**, 1130 (2003).
- [18] B. Nonas, I. Cabria, R. Zeller, P. H. Dederichs, T. Hühne, and H. Ebert, Phys. Rev. Lett. **86**, 2146 (2001).
- [19] B. Lazarovits, L. Szunyogh, and P. Weinberger, Phys. Rev. B **65**, 104441 (2002).
- [20] J. Dorantes-Dávila and G. M. Pastor, Phys. Rev. Lett. **81**, 208 (1998).
- [21] R. Félix-Medina, J. Dorantes-Dávila, and G. M. Pastor, Phys. Rev. B **67**, 094430 (2003).
- [22] M. D. Stiles, S. V. Halilov, R. A. Hyman, and A. Zangwill, Phys. Rev. B **64**, 104430 (2001).
- [23] H. J. Jansen, Physics Today **48**, 50 (1995).
- [24] J. C. Slater and G. F. Koster, Phys. Rev. **94**, 1498 (1954).
- [25] H. M. Duan and Q. Q. Zheng, Phys. Lett. A **280**, 333 (2001).
- [26] W. Wernsdorfer, E. B. Orozco, A. Benoit, D. Mailly, O. Kubo, H. Nakamo, and B. Barbara, Phys. Rev. Lett. **79**, 4014 (1997).
- [27] P. Bruno, Phys. Rev. B **39**, 865 (1989).
- [28] A. Cehovin, C. M. Canali, and A. H. MacDonald, Phys. Rev. B **69**, 045411 (2004).
- [29] C. T. Chen, Y. U. Uzerda, H. J. Lin, N. V. Smith, G. Meigs, E. Chaban, G. Ho, E. Pellegrin, and F. Sette, Phys. Rev. Lett. **75**, 152 (1995).
- [30] W. A. Harrison, *Electronic structure and the properties of solids* (Dover, New York, 1988).
- [31] J. Y. Park, J. H. Seo, C. N. Whang, S. S. Kim, D. S. Choi, and K. H. Chae, Bull. Am. Phys. Soc. **50**, 257 (257).
- [32] This is the case also for the system with the largest anisotropy energy found so far [17], namely a single cobalt atom adsorbed on a platinum surface, which has a MAE of 9 meV, more than three orders of magnitude larger than in bulk